Earth Planet. Sci. Lett. 630 (2024) 118615

Contents lists available at ScienceDirect

Earth and Planetary Science Letters

journal homepage: www.elsevier.com/locate/epsl

Impact of mantle convection and dynamic topography on the Cenozoic paleogeography of Central Eurasia and the West Siberian Seaway

Eivind O. Straume [a,b,*], Bernhard Steinberger [c], Thorsten W. Becker [a,d], Claudio Faccenna [c,e]

[a] UTIG & EPS at the Jackson School of Geosciences, UT Austin
[b] NORCE Norwegian Research Centre AS & the Bjerknes Centre for Climate Research, Bergen, Norway
[c] GFZ German Research Center for Geosciences, Germany
[d] Oden Institute for Computational Engineering & Sciences, UT Austin
[e] University Roma TRE, Italy

ARTICLE INFO

Editor: Dr H Thybo

Keywords:
Paleogeography
Oceanic gateways
Mantle convection
Dynamic topography
Paleoclimate
Geodynamics

ABSTRACT

The West Siberian Seaway connected the Tethys to the Arctic Ocean in the Paleogene and played an important role for Eurasian-Arctic biogeography, ocean circulation, and climate. However, the paleogeography and geological mechanisms enabling the seaway are not well constrained, which complicates linking the seaway evolution to paleoenvironmental changes. Here, we investigate the paleogeography of the Peri-Tethys realms for the Cenozoic time (66–0 Ma), including the West Siberian Seaway, and quantify the influence of mantle convection and corresponding dynamic topography. We start by generating continuous digital elevation models for Eurasia, Arabia, and Northern Africa, by digitizing regional paleogeographic maps and additional geological information and incorporate them in a global paleogeography model with nominal million-year resolution. Then we compute time-dependent dynamic topography for the same time interval and find a clear correlation between changes in dynamic topography and the paleogeographic evolution of Central Eurasia and the West Siberian Seaway. Our results suggest that mantle convection played a greater role in Eurasian paleogeography than previously recognized. Mantle flow may have influenced oceanic connections between the Arctic and global ocean providing a link between deep mantle convection, surface evolution, and environmental changes. Our reconstructions also indicate that the Arctic Ocean may have been isolated from the global ocean in the Eocene, even if the West Siberian Seaway was open, as the Peri-Tethys – Tethys connection was limited, and the Greenland-Scotland Ridge was a landbridge.

1. Introduction

Plate tectonics, mantle dynamics, volcanism, and eustasy controlled the Cenozoic (66 – 0 Ma) paleogeography of the Peri-Tethys realms and affected reorganizations in biogeography, ocean circulation, and climate. The West Siberian Seaway (WSS), encompassing the Turgai Strait, West Siberian Sea, and the Kara Strait, provided a shallow water connection over northern Eurasia linking the Tethys and Arctic Ocean in the Paleogene (Fig. 1). At this time, Eurasia was covered by an epicontinental sea which was a part of the Peri-Tethys that included flooded platform areas on either side of the Arabia-Eurasia convergence zone (Meulenkamp and Sissingh, 2003). The epicontinental sea was connected to the Tethys in the south during most of the Paleogene, then sometimes referred to as the proto-Paratethys Sea, until the Late Eocene when continent collision closed the Tethys-Peri-Tethys connections resulting in the origin of the isolated Paratethys Sea (Bosboom et al., 2017; Meulenkamp and Sissingh, 2003; Rögl, 1999). It is suggested that this sea reached to the Arctic Ocean through the Turgai Strait and West Siberian Sea, and at its most extensive, the WSS likely enabled an ocean corridor between the Arctic and Tethys Oceans.

Previous studies suggest the seaway was open in the Latest Cretaceous/Early Paleocene, then closed sometime in the Paleocene (Barrier et al., 2018; Brikiatis, 2014), opened again around the Paleocene-Eocene, and stayed open throughout the Eocene until in closed permanently by the Late Eocene (Akhmetiev et al., 2012; Barrier et al., 2018; Rögl, 1997). However, the timing and configuration of the Eurasian-Arctic connections is not well constrained and while some studies indicate the seaway may have been operational in for most of the

* Corresponding author at: NORCE Norwegian Research Centre AS, Jahnebakken 5, 5007 Bergen, Norway
E-mail address: eist@norceresearch.no (E.O. Straume).

https://doi.org/10.1016/j.epsl.2024.118615
Received 11 May 2023; Received in revised form 28 January 2024; Accepted 6 February 2024
Available online 17 February 2024

Eocene (Akhmetiev and Beniamovski, 2009; Akhmetiev et al., 2012), others have the Arctic connection closed continuously or periodically during this time (Barke et al., 2011; Blakey, 2021; Kaya et al., 2019; Palcu and Krijgsman, 2022), or closed but prone to episodic flooding due to second order sea level changes (Iakovleva et al., 2001). This includes possible restrictions in the Kara Strait, north of the West Siberian Sea, that could have inhibited a connection to the Arctic already in the Early – Mid Eocene even if the Turgai Strait was open (Kaya et al., 2019; Palcu and Krijgsman, 2022). The suggested timing of the final closure of the Arctic-Tethys seaway also ranges in the literature form Mid Eocene (Palcu and Krijgsman, 2022) to Early Oligocene (Rögl, 1997), which makes it challenging to link the closure to specific paleo-environmental events in the Cenozoic.

Constraining the evolution of the WSS is thus very important as it would have implications for ocean circulation, climate, and biogeographic dispersal of marine and terrestrial species. For example, it is proposed that the WSS contributed to the meridional heat transport from tropical to high latitudes during the global warming at the Paleocene-Eocene Thermal Maximum (PETM) (Akhmetiev et al., 2012), and that a later reduction in the flow through the WSS and the Tethys-Paratethys connections advanced a subtropical Monsoon climate over North Central Eurasia (Akhmetiev and Beniamovski, 2009). Also, recent modelling studies (i.e. Hutchinson et al., 2019; Straume et al., 2022) show that the salinity of the Arctic Ocean, which would depend on the paleogeography of the WSS, played a critical role for the Atlantic Overturning and global climatic changes in the Late Eocene and during the Eocene-Oligocene Transition.

The WSS was located over the West Siberian Basin which is the largest cratonic basin in the world (Allen and Armitage, 2011). The basin formed after the Permo-Triassic uplift event related to plume arrival beneath the lithosphere and the following emplacement of the Siberian trap basalts (Reichow et al., 2005; Saunders et al., 2005), and

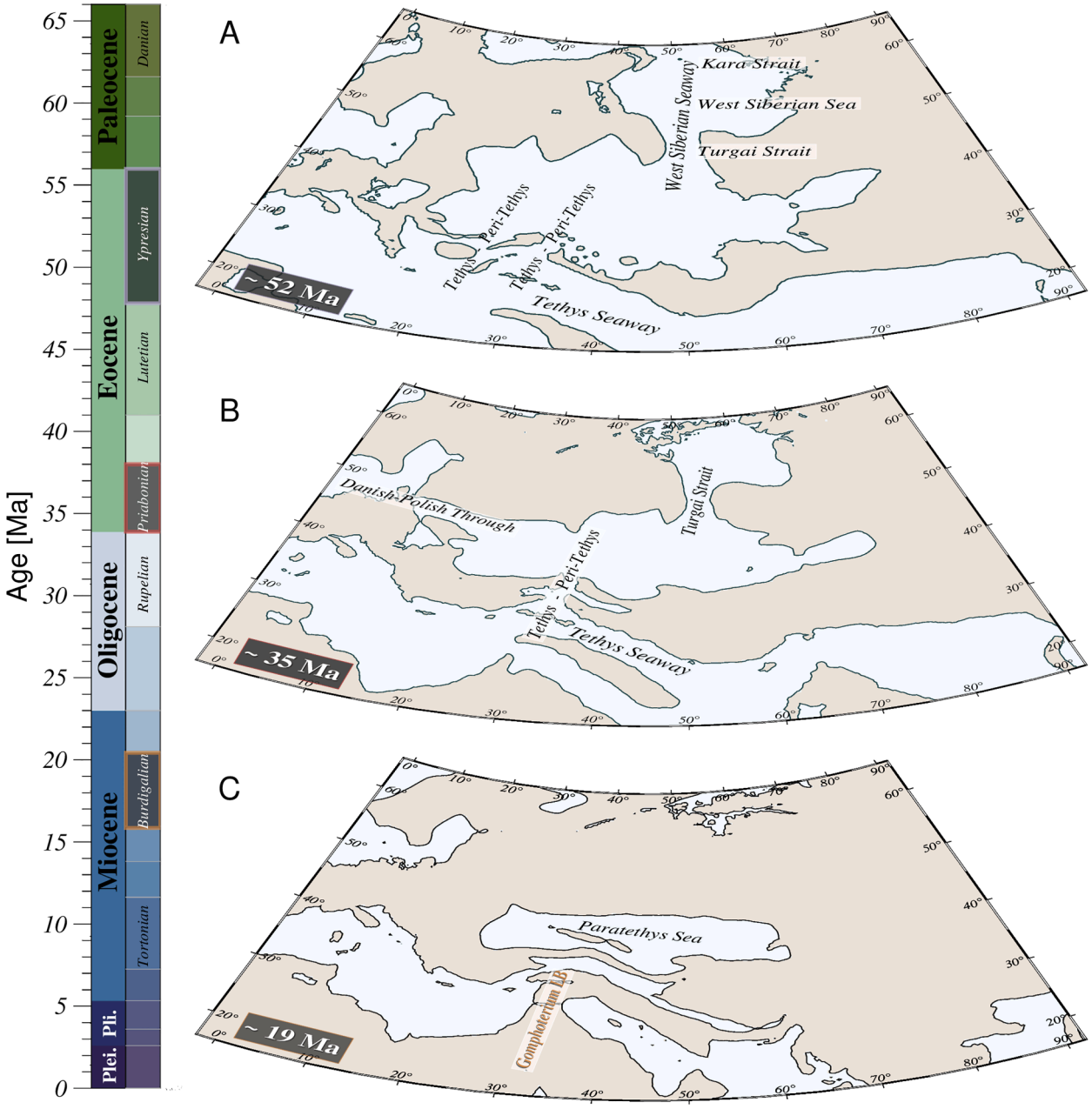

Fig. 1. Simplified paleogeography maps of Eurasia and the Peri-Tethys region for different Cenozoic time steps. A) Ypresian (~52 Ma). B) Priabonian (~35 Ma). C) Burdigalian (~19 Ma). Light grey = ocean, dark grey = land. We only name the Cenozoic stages described in the text.

evolved with succeeding periods of subsidence recorded from the Jurassic (~200 Ma) until the Oligocene (~30 Ma) (Vibe et al., 2018; Vyssotski et al., 2006). This prolonged subsidence has been linked to continued lithospheric stretching and thinning (Armitage and Allen, 2010), which was an important prerequisite for the original location of the seaway, but this process was largely completed by the Cretaceous (Vyssotski et al., 2006) and cannot explain paleogeographic changes in the Cenozoic. Also, episodes of uplift, which must be explained by other mechanisms, are recorded in the Mesozoic and Cenozoic (Vetrov et al., 2021; Vibe et al., 2018). Quantifying the mechanisms and geological processes at play in Central Eurasia during the Cenozoic is crucial and may provide better constraints to the Evolution of the WSS. Tectonic forces and global sea level changes are often used to explain the WSS paleogeography. However, Northern Central Eurasia likely experienced little tectonic activity during this time (e.g., Glorie and De Grave, 2016), and although eustacy played an important role, the global sea level changes cannot alone account for the extent of the WSS (Popov et al., 2010). A configuration resembling that of previous Paleogene reconstructions (Akhmetiev et al., 2012), would (if sea level was the only factor) require more than 200 m higher sea level than today. This would be consistent with the most extreme sea level estimates for the Paleogene (e.g., Haq and Al-Qahtani, 2005; Haq et al., 1987; Xu et al., 2006), but would also flood most of Northern Eurasia between Scandinavia and the Urals providing a more significant sea/seaway to the Arctic Ocean west of the Urals, for which there is little evidence. However, a narrow strait is sometimes inferred along the western flank of the Urals (i.e., Akhmetiev and Beniamovski, 2009; Akhmetiev et al., 2012; Beniamovski, 2007). This suggests that other mechanisms, such as mantle convection and corresponding changes in dynamic topography likely influenced the paleogeography of the seaway (Vibe et al., 2018).

In this paper, we explore the role of mantle convection and dynamic topography on the paleogeographic evolution of the Peri-Tethys realms including the WSS. We do this by generating a new continuous Cenozoic digital elevation model (DEM) for Eurasia, Arabia, and Northern Africa based on geological evidence primarily from the tectono-sedimentary-palinspastic maps of Barrier et al. (2018). The new DEMs are then incorporated in the paleogeography model of Straume et al. (2020), to create new global Cenozoic DEM from 66 Ma to present. In addition, we compute new global time-dependent dynamic topography reconstructions based on recent plate motions and tomography models and investigate the correlation between mantle convection and changes in paleogeography. Lastly, we evaluate the role of the mantle convection and paleogeography on oceanographic, climatic, and biogeographic events in the Peri-Tethys realms during the Cenozoic time.

2. A new Cenozoic paleogeographic digital elevation model for Eurasia, Arabia, and Northern Africa

Detailed paleogeographic digital elevation models (DEMs) are essential to study past climates and are one of the most important boundary conditions in deep time paleo-ocean circulation and climate models. This is our motivation for generating a new continuous Cenozoic DEM for the Tethyan realm including Northern Africa, Arabia, and Eurasia, based on the Tectono-Sedimentary-Palinspastic maps of Barrier et al. (2018). Additionally, we make adjustments to key regions such as the Tethys and West Siberian Seaways considering published regional paleogeographic indicators such as: Geological/sedimentary data which we used to constrain the outlines of the WSS north of our main study area in the Eocene (e.g., Akhmetiev et al., 2012), biogeographic data on terrestrial biota migrations which were used as indications of a closed seaway in the Early Paleocene (e.g., Brikiatis, 2014), and oceanographic data indicating periodically continuous connection to the Arctic Ocean in the Eocene (e.g., Dickson et al., 2022). The reconstructions are ultimately incorporated in the global model of Straume et al. (2020) creating a new global paleogeographic DEM for every millionth year of the Cenozoic time.

The general methodology of the paleogeographic reconstructions is as outlined in Straume et al. (2019) (oceanic domain) and Straume et al. (2020) (oceanic + continental domain), but the models for the continental topography in the Peri-Tethys realm include a new approach of digitizing geological units of the past and approximating elevation based on the type of environment. We take advantage of the Tectono-Sedimentary-Palinspastic maps of Barrier et al. (2018) which cover the Peri-Tethys realms for several time intervals in the Cenozoic including the Danian (66.0–61.6 Ma), Ypresian (56–47.8 Ma), Lutetian (47.8–41.2 Ma), Priabonian (37.8–33.9 Ma), Rupelian (33.9–27.8 Ma), Burdigalian (20.4–16.0 Ma), and Tortonian (11.6–7.2 Ma). We digitize and convert these maps to elevation for each time slice using approximate elevations outlined in Table 1.

Overall, this gives a good first order approximation of the elevation, but there are uncertainties in estimating the exact elevation in deep time based on this methodology, primarily as the geological maps do not constrain exact elevation and do not cover the Cenozoic continuously. We strive to minimize these uncertainties by evaluating tectonic setting, sea-level, present-day topography, and other reconstructions, to make our model as realistic as possible. We apply this methodology for Eurasia, Arabia, and Northern Africa separately to rotate the resulting grids with their respective plate motion path in a paleomagnetic reference frame. To cover the time gaps between the digitized maps we blend the grids using cosine taper weights, by applying a *Generic Mapping Tools* (Wessel et al., 2019) grid blending module. We change the weighting for each time step, so when, e.g., generating the 40 Ma paleogeography (in the gap without data between the Lutetian and Priabonian reconstructions) the resulting grid is a blend of the Lutetian and Priabonian digitized grids with a stronger weighting of the Lutetian which is closer in time to 40 Ma. We apply this before moving the grids to their paleo-location so that the blending routine is not influenced by any tectonic lateral motion (See supplementary Figs. S1-S3 for reconstructed topography at present location). Where we have additional data for specific regions or other timesteps, we adjust the models manually at the respective locations and/or time intervals. Lastly, the new reconstructions are incorporated in the Straume et al. (2020) model, making a new global Cenozoic paleogeography DEM (Fig. S5).

Our paleogeography is reconstructed using a paleomagnetic reference frame to be applicable for paleoclimate. Paleomagnetic reference frames are relative to the Earth's spin axis, the latitude from which determines solar energy and the climatic zones (e.g. Lithgow-Bertelloni and Gurnis, 1997; Torsvik et al., 2008; van Hinsbergen et al., 2015). In contrast, mantle/hotspot reference frames are relative to the deep mantle and are useful for geodynamic questions but are not intended for paleoclimate studies. In particular, mantle reference frames, with some

Table 1
Conversion from paleo-geological environment to elevation. Classes and environments names as in Barrier et al. (2018).

Class	Environment	Elevation
Continental	High-moderate mountains, active mountain ranges	> 2000 m
	Low mountains and plateaus	500 m–1500 m
	Lowland, erosional plains	100 m–400 m
	Fluvio-lacustrine, Alluvial plains, Continental molasse	0 m–200 m
Transitional	Flooded lowland/Marginal marine, Coastal plain/ Shallow mixed shelf, Deltaic fan, Evaporites	–50 m–50 m
Marine	Reef, carbonate, and terrigenous platforms	–300 m—100 m
	Slope/basinal deeper marine carbonates and clastics, radiolarites	–1500 m—400 m
	Deep marine sediments	< –2000 m

The given range in elevations reflects variations along slopes such as continental margins and roughness inherited from the present-day topography. The final elevation in the DEMs is also influenced by the tectonic model and therefore differ in some places, manly in the vicinity of plate boundaries.

exceptions (e.g., Müller et al., 2022), exclude true polar wander which is the mean rotation of both crust and mantle relative to the spin axis arising from redistribution of density heterogeneities in the mantle and corresponding changes in the Earth's moment of inertia (Goldreich and Toomre, 1969; Steinberger and Torsvik, 2010; Torsvik et al., 2012). Used inappropriately, mantle reference frames can yield considerable paleolatitude errors (e.g., van Hinsbergen et al., 2015)–more than 10° for the Cenozoic, and even larger further back in time.

We re-emphasize the need to use a paleomagnetic reference frame because the majority of previous paleo-climate model studies appears to be on mantle reference frames. For example, the Deep-Time Model Intercomparison Project (DeepMIP) has mainly used the Herold et al. (2014) mantle frame reconstruction for the Early Eocene. Where only one out of eight climate models analyzed for the DeepMIP Early Eocene study of Lunt et al. (2021) used a paleomagnetic reference frame reconstruction and none of the nine models used for the Early Eocene analysis of African climate by Williams et al. (2022) used a paleomagnetic reference frame.

2.1. Eurasia and the West Siberian Seaway

We reconstruct the paleogeography of Eurasia, including the WSS, following the methodology described above based on the maps of Barrier et al. (2018). This does not cover Eurasia entirely, but a region that today spans between ~ 20°E–105°E and ~ 20°N–60°N (Fig. 2). It includes Eastern Europe in the West, the Himalayas and Tibetan Plateau in the East, the Eurasian continent boundary in the South, and Siberia in the North. The parts of Eurasia outside this region are reconstructed as in Straume et al. (2020), where the continental parts north of 60°N are reconstructed after the pre-glacial topography model of Medvedev et al. (2018) and global sea level changes, while the few remaining regions not updated here keep the present day elevation adjusted for sea level changes rotated to their paleo-location. Our model diverges from the maps of Barrier et al. (2018) as we use a different plate tectonic model, especially influencing the elevation along the southern margin of Eurasia due to different configuration and timing of the Arabia-Eurasia continent collision. We use the rotations of Torsvik et al. (2019) and a modified version of the continental polygons of Torsvik and Cocks (2016), with new continent-ocean boundaries for Eurasia and Arabia modified from van Hinsbergen et al. (2020) and optimized for paleogeographic reconstructions by Straume et al. (2020). We also add the Bitlis Massif from the kinematic model of van Hinsbergen et al. (2020) to improve the model for the Tethys Seaway (see below), which also influences/improves the reconstructions of southern Eurasia.

For the WSS in the Cenozoic, our reconstructions show a closed seaway in the Paleocene (66–56 Ma), an open but shallow seaway in the Eocene (56 – 33.9 Ma), and a closed seaway afterwards. This is consistent with other reconstructions of the seaway (Akhmetiev et al., 2012; Barrier et al., 2018). It contradicts some studies having the seaway closed in the Early – Mid Eocene time (Barke et al., 2011; Blakey, 2021;

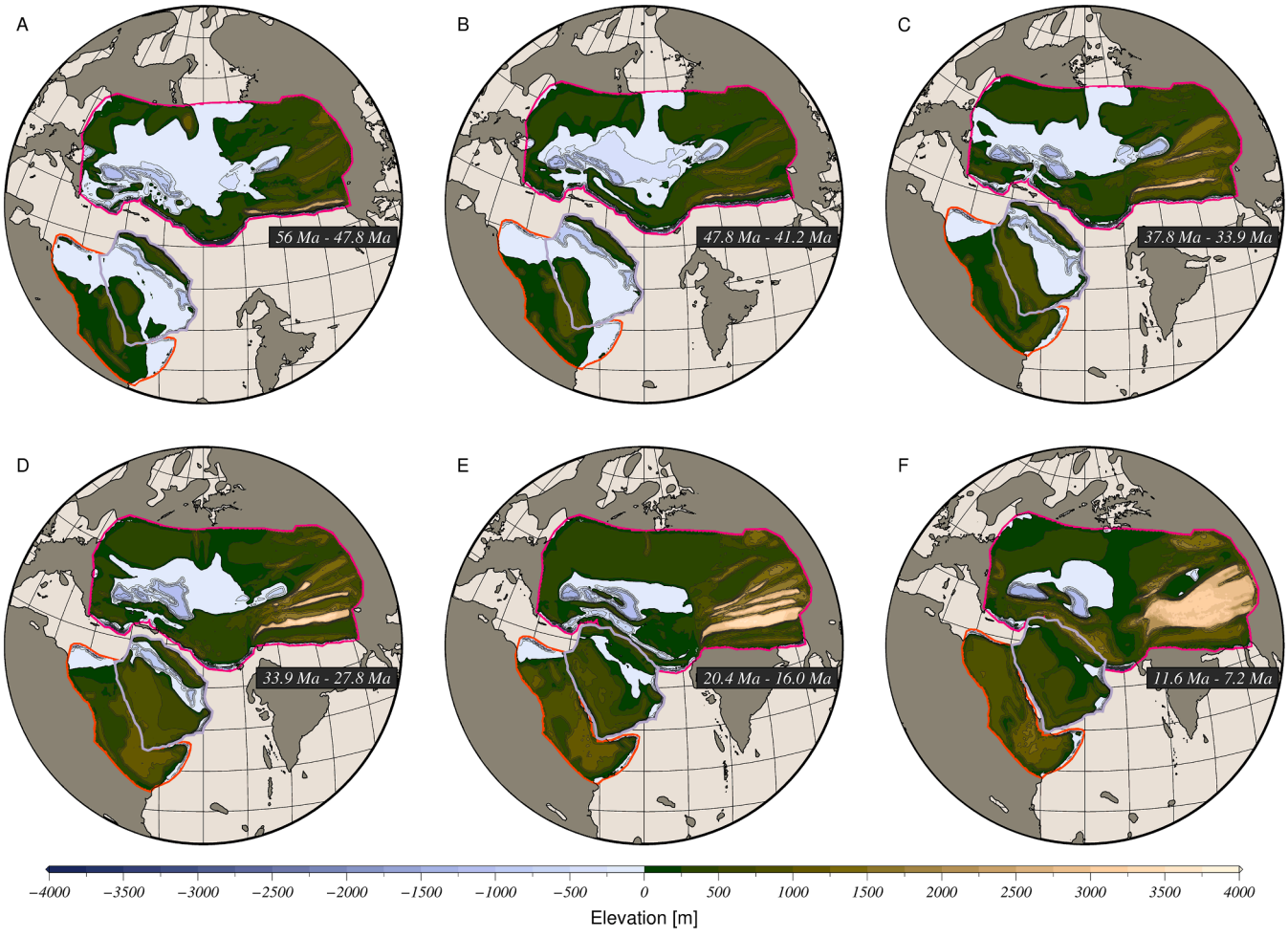

Fig. 2. Eurasian (outlined in pink), Arabian (lavender), and North African (orange) paleogeography constructed by digitizing the Tectono-Sedimentary-Palinspastic maps of Barrier et al. (2018) and incorporated in the plate tectonic kinematic model of Torsvik et al. (2019). We show the reconstructions from: A) Ypresian (56 Ma – 47.8 Ma), B) Lutetian (47.8 Ma–41.2 Ma), C) Priabonian (37.8 Ma – 33.9 Ma), D) Rupelian (33.9 Ma – 27. 8 Ma), E) Burdigalian (20.4 Ma–16.0 Ma), F) Tortonian (11.6 Ma – 7.2 Ma). See Fig. S4 in the supplementary material for the Danian (66.0 – 61.6 Ma) maps, these are also included in our model, but are not shown here.

Palcu and Krijgsman, 2022), however, the seaway in our model is very shallow and prone to close from changes in sea level like suggested by Iakovleva et al. (2001) during this time, and we cannot rule out an early closure of the Kara Strait as suggested by Palcu and Krijgsman (2022).

2.2. Arabia and Northeast Africa

Like Eurasia, Arabia was flooded by an epicontinental sea in the early Cenozoic, but due to elevation changes caused by the plate tectonic rifting and collision with Eurasia, eustacy, and changes in dynamic topography, the continent gradually emerged above sea level by Late Miocene times (Fig. 2). We reconstruct the Arabian paleogeography after the maps of Barrier et al. (2018); however, we also modify our reconstructions in between the Burdigalian (20.4–16.0 Ma) and Tortonian (11.6–7.2 Ma) to allow for a re-opening of a shallow seaway after the first appearance of the *Gomnphoterium* landbridge (Fig. 1) in the Early Burdigalian (see section on the Tethys Seaway below). This is based on marine species migration and geological evidence suggesting a temporal re-establishment of a shallow marine seaway in the Mid Miocene (~ 16–12 Ma) connecting the Mediterranean with the Indian ocean over a flooded Arabia (e.g. Bialik et al., 2019; Segev et al., 2017).

We reconstruct Northeast Africa separately from Arabia although separation, through seafloor spreading in the Red Sea, did not start before the Miocene, at ~13–12 Ma (Augustin et al., 2021). However, doming related to the arrival of the Afar Plume (centered near Ethiopia and Yemen) instigated an initial phase of African – Arabian rifting in the Early Oligocene sometime between ~ 34 Ma–32 Ma (e.g., Collet et al., 2000; Segev et al., 2017), which caused relative motion between Africa and Arabia from that time. The Northeast African reconstructions are generated from the maps of Barrier et al. (2018), but as with Arabia and Eurasia the locations differ due to the updated tectonic kinematic model, and topography in the vicinity of plate boundaries are also influenced by the paleogeography model.

2.3. Tethys seaway

Before the Arabia-Eurasia collision, the Tethys Seaway was a deep oceanic gateway linking the Indo-Pacific and Atlantic Oceans. The closure of the Tethys Seaway is recognized as an important step towards the modern ocean circulation and climate, and has been suggested to facilitate the transition towards a stronger overturning circulation in the North Atlantic Ocean (Zhang et al., 2011), influence upwelling in the Arabian Sea which could have strengthened the South Asian Monsoon (Bialik et al., 2019), and even to affect the strength of the Antarctic Circumpolar Current, by ending transport of warm saline Mediterranean waters to the Indian ocean continuing as far south as the Southern Ocean (Hamon et al., 2013; Ramsay et al., 1998).

Here, we reconstruct the paleobathymetry of the oceanic lithosphere in the seaway using the methodology outlined in Straume et al. (2020), but also adding tectonic units of the Bitlis Massif from van Hinsbergen et al. (2020), which blocks parts of the Seaway before continent collision. The first closure of the seaway has been suggested to coincide with the consumption of the last remaining Eastern Tethys oceanic lithosphere (Okay et al., 2010). However, our kinematic model and the new continental reconstructions of Arabia and Eurasia show the oceanic part close at ~ 30 Ma, 10 Myr before full closure of the Tethys Seaway, and that final closure of the seaway, with the emergence of the "Gomphoterium landbringe" (Rögl, 1997) occurred across the flooded Arabian continent after the initial stages of continent collision. There are geological indicators for a re-opening of a shallow seaway in the Mid Miocene (~16–12 Ma) across Arabia (e.g. Bialik et al., 2019; Segev et al., 2017), and as mentioned in the previous section, we incorporate this in our reconstructions in between the Burdigalian and Tortonian reconstructions.

3. Cenozoic mantle convection and dynamic topography models

3.1. Methodology

We investigate the role of mantle convection on surface paleotopography using an updated version of the global mantle convection modelling routine discussed in Steinberger et al. (2004). This approach computes time-dependent dynamic topography by advecting mantle density anomalies backward in the mantle flow field, based on mantle densities from present-day inferred from seismic tomography and surface plate velocities. Similar computations have been explored before, and here we mostly follow a procedure as described in Müller et al. (2008): We convert relative seismic share wave velocity to relative density anomalies by scaling with a factor 0.25 and exclude any anomalies above 200 km depth. To compute past anomalies, we use both "pure backward advection", leading to anomalies also in the uppermost 200 km in the past, and "modified backward advection" where mostly cold, sinking anomalies in the uppermost 200 km are removed, and mostly hot, rising anomalies are upward-continued to depth 200 km. Our models benefits from updates using more recent tomography where we mainly use SMEAN2 (Jackson et al., 2017) and Tx2019slab (Lu et al., 2019), but also testing S40RTS (Ritsema et al., 2011) and SEMUCB-WM1 (French and Romanowicz, 2014). In addition, we use new plate velocities derived from Torsvik et al. (2019) and besides the mantle viscosity structure of Steinberger and Calderwood (2006) we use the updated mantle viscosity structure of Steinberger (2016).

Our paleogeographic DEMs are intended for paleoclimate studies, where the climate system depends on latitude from rotation pole, and therefore reconstructed using a paleomagnetic reference frame. Therefore, our time-dependent dynamic topography should also be in a paleomagnetic reference frame to accurately compare through time. This is achieved as follows: For backward-advecting mantle density anomalies, we use a mantle reference frame. By replacing the free-slip boundary condition at the core-mantle-boundary (CMB) with no-slip for degree 1 toroidal only, we allow for a net rotation of plate motions over the relatively fixed lower mantle, in the absence of lateral viscosity variations. Backward-advection is done here back to 100 Ma but, as is well known, becomes increasingly unreliable further back in time. In particular, the computed density field becomes successively more layered, and flow speeds decrease further back in time.

In the next step, these backward-advected density anomalies for each reconstructed timestep are used to compute surface stress, with a free-slip (instead of prescribed plate motions) boundary condition at each instance, which is converted to dynamic topography "beneath air" using a density contrast 3300 kg/m^3 between uppermost mantle and air. Lastly, the resulting dynamic topography fields are transferred into the paleomagnetic frame with finite rotations also specified in Torsvik et al. (2019), corresponding to true polar wander. We also provide our dynamic topography estimates in an alternative, mantle reference frame (see data availability statement).

3.2. Results

The resulting time-dependent dynamic topography and mantle flow predictions are shown in Figs. 3, 5, and S6-S8. We focus our discussion on results computed using the SMEAN2 composite tomography but results from other tomographic models are shown in the supplementary (and data are made available). The different model runs show similar predictions in terms of amplitude, where peak-to-peak ranges around ± 2 km, with results for TX2019 slightly lower (closer to ± 1.5 km), and SEMUCB-WM1 slightly higher (closer to ± 2.5 km). These ranges are comparable with estimates from previous work (see e.g., Flament et al., 2013, for a review) but amplitudes depend on the specific modeling setup, and there is some debate as to what dynamic signal is compatible with constraints on residual topography (e.g., Hoggard et al., 2016; Yang et al., 2017).

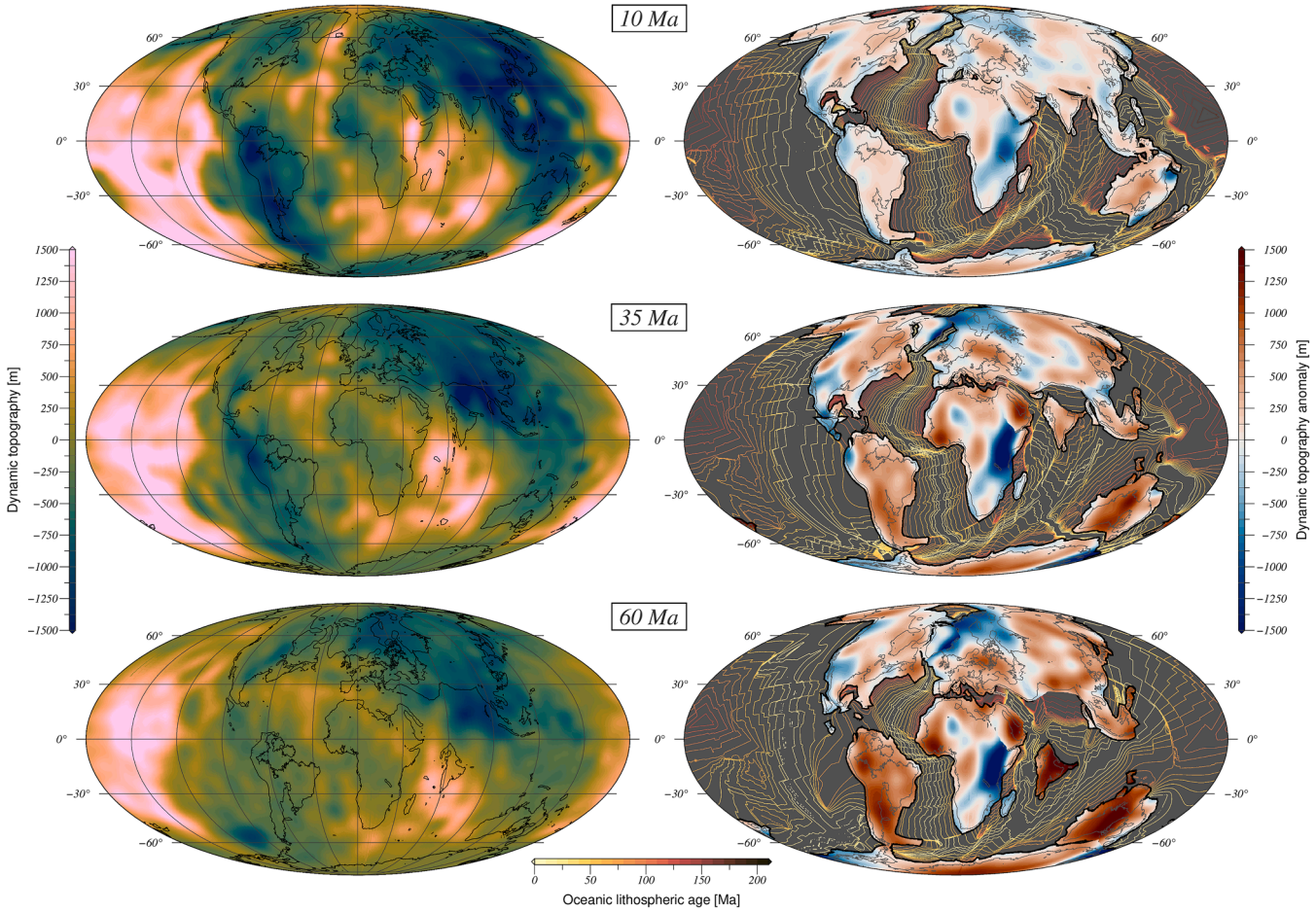

Fig. 3. Dynamic topography computed using SMEAN2 tomography and plate velocities of Torsvik et al. (2019). Left panels show dynamic topography predictions, and right panels show the difference between the paleo-dynamic topography (for10 Ma, 35 Ma, and 60 Ma) and the present dynamic topography rotated to its paleo-location, in order to highlight the change in continental dynamic topography. The right panels also show oceanic lithospheric ages (Straume et al., 2020) that are used in reconstructing paleobathymetry. See text for further explanations.

The general issue of dynamic topography amplitudes aside, we are here mainly concerned with temporal change of dynamic topography. For this, we exclude density anomalies in the upper 200 km, as they either do not lead to changes in dynamic topography, if they are within the lithosphere, or corresponding temporal changes are hard to predict for more than a few million years back in time, due to small-scale convection in the low-viscosity asthenosphere and the effects of thermal diffusion which cannot be time-reversed. Amplitude predictions from our backward convection reconstructions decrease back in time as the computed density fields become more layered, and flow speeds decrease.

Spatially, the dynamic topography depends somewhat on which tomographic models are considered (Figs. 3, 5, and S6-S11) but the patterns are overall similar in important regions were the structural models agree. On the largest scales, all models show the long wavelength, degree 2 pattern with highs over Africa and the Pacific Ocean, and circum-Pacific lows (Flament et al., 2013), and those serve to organize regional flow patterns. On smaller scales, all models considered show a negative anomaly over the West Siberian Sea back in time, for example. Focusing on Central Eurasia, and Cenozoic changes in dynamic tomography, we favor the models that are based on the most recent tomographic imaging (i.e., SMEAN2 and TX2019) because we have found those models to also provide good model fits to present-day indicators of dynamic consistency, e.g., by comparison with geoid and plate motion predictions. However, the spatial correlation with the evolution of the WSS is not as clear when using the older models (i.e., S40RTS and SEMUCB-WM1), as further discussed below.

4. Discussion

4.1. The West Siberian Seaway and dynamic topography

To investigate how changes in dynamic topography may have affected the surface topography through time, we compute the difference between the present-day and paleo-dynamic topography (Fig. 3, right panels). The present dynamic topography is rotated to the paleo-location before calculating the difference so that the resulting dynamic topography anomaly represents how much the present topography would have changed from changes in dynamic topography, accounting for the tectonic motion of the continents. Notably, for the Paleogene, we observe a clear negative anomaly over Eurasia that correlates well with our reconstructed paleogeography of the WSS (Figs.3 & 4) based geological evidence (i.e., Barrier et al., 2018). This correlation is most significant in our models using Tx2019 and SMEAN2 tomography, but a similar pattern is also observed in our models using the older tomography models where all models tested in this study yield a negative dynamic topography anomaly back in time in the West Siberian Sea. However, S40RTS (Figs.S7 & S10) and SEMUCB-WM1(Figs. S8 & S11) do not show a negative anomaly around the paleo-location of the Turgai Strait (see supplementary material for details). These changes indicate uplift in West Siberia due to dynamic topography in the interval from the Paleogene towards the present which is in agreement with the recorded

subsidence history of the basin based on stratigraphic data (Vibe et al., 2018). It is also observed in the circum-Arctic dynamic topography models of Shephard et al. (2014), but is in contrast to the computations of Spasojevic and Gurnis (2012) who model a west-east tilting of Siberia.

The model of Shephard et al. (2014), like many previous similar models, differs from our estimates of dynamic topography over time because it is based on plate reconstructions and subduction history alone, and not on back-tracking seismic tomography. This means that while slab-induced negative dynamic topography may be captured in such models, dynamic topography highs are only associated with broad-scale return flow. Therefore, such models do not have a focused dynamic topography high in Afar, for example. A subduction centric modeling approach has its merits, in particular when going further back in time, beyond the ~60 Myr limit when the backward-advection becomes unreliable, and when results are calibrated against tomography to understand slab trajectories (e.g., Conrad and Gurnis, 2003).

However, we regard our approach more suitable and complete for the geologically more recent past which we are concerned with here. The approach of Spasojevic and Gurnis (2012) used hybrid geodynamic models that combine inverse with forward models to overcome their individual limitations. Their approach considers both tomography and plate reconstructions and, in this way, is more like ours. The difference between their predictions and ours for central Eurasia is likely the result of using different seismic tomography models, since we also find considerable differences for our own results when using different tomography models. The dynamic topography results presented here are spatially more in agreement with the reconstructed paleogeography of the WSS than the previous paleo-dynamic topography models, which likely results from using more recent tomography models (e.g., SMEAN2 and Tx2019) that arguably better image the seismic velocity anomalies below central Eurasia. In future work, further progress may be achieved by updating the hybrid models developed by Spasojevic and Gurnis

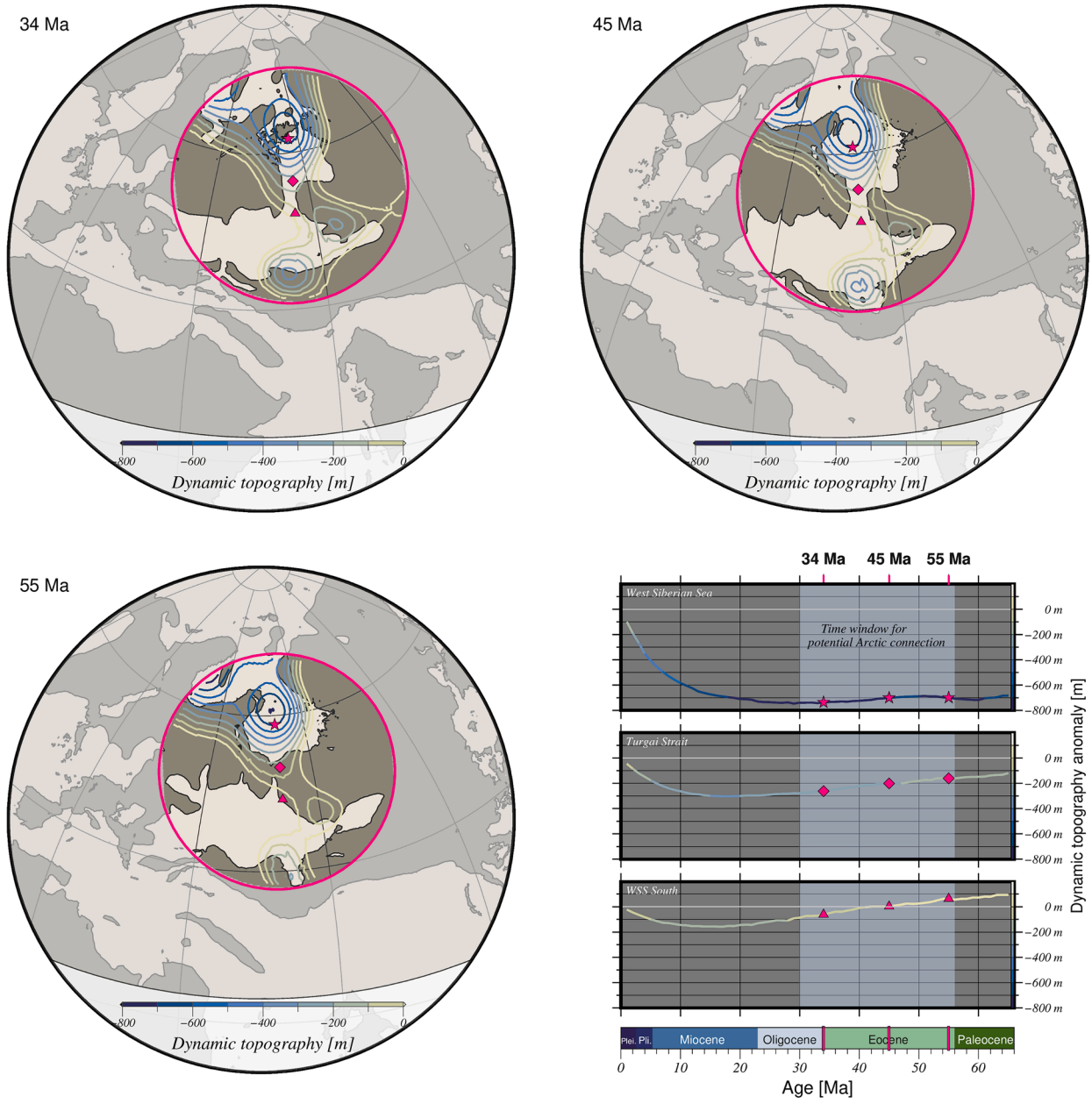

Fig. 4. Negative dynamic topography anomalies over North Central Eurasia during the Eocene. The maps show the negative dynamic topography anomaly over central Eurasia (see text for details), plotted on top of the paleogeography reconstructed in this paper (grey = land, light beige = water). This figure shows the results computed using the SMEAN2 tomography model (the other models are shown in the supplementary, Figs. S9-S11).

(2012) with more recent topography models and plate reconstructions.

The explanation for this dynamic topography anomaly is changes in a slow seismic anomaly beneath North Central Eurasia, originating at the core mantle boundary, that is inferred to be an active upwelling forward in time, and hence advected down in the mantle back in time (Fig. 5.). Backward advection of the slow anomaly influences the computed dynamic topography and gives rise to the negative dynamic topography anomaly in Fig. 4. This seems to be part of a larger convection cell, where the upwelling beneath Eurasia may be triggered by the downwelling corresponding to the sinking slabs associated with the Tethyan subduction (Fig. 5). These changes in mantle flow and corresponding dynamic topography could explain the topographic evolution of the WSS in the Paleogene.

The computed dynamic topography is up to 800 m lower over Northern Eurasia in the West Siberian Sea region during the Eocene, indicating the potential for a significantly deeper basin in the Early Cenozoic. A deeper basin in the past is supported by apatite fission track thermochronology indicating uplift in the West Siberian Basin (Vetrov et al., 2021). However, the exhumation ceased by the Cretaceous, before the time we are considering. The fission track study of Vetrov et al. (2021) also record Cenozoic uplift and link this exhumation history to far-field effects from tectonic activity along the southern and eastern margins of Eurasia. However, this is for Novosibirsk massif which is closer to the regions influenced Indian-Eurasian collision and seems less likely as an explanation for the paleogeographic changes in our study area as most of the West Siberian Sea was far away from any plate boundary throughout the Cenozoic. Also, the tectonic subsidence of the West Siberian Basin presumably ended earlier (Vyssotski et al., 2006) so processes such as decreasing lithospheric stretching were not influencing the paleogeography during the time we are considering here. Our model indicates that mantle convection and changes in dynamic topography may be a more likely explanation. This would have been most significant North of the Turgai Strait, and far field tectonic effects from the Indian-Asia or Arabia- Eurasia collisions could still have played a role further South, i.e., for the evolution of the proto-Paratethys sea (e.g., Kaya et al., 2019). The topography anomaly is weaker around the paleo-location of the Turgai Strait (with maximum differences ~200 m), supporting the view that the Peri-Tethys-Arctic connections were likely shallow as suggested by previous paleogeographic reconstructions (e.g., Akhmetiev et al., 2012; Barrier et al., 2018). Also, that a combination of sea level changes, tectonics, and dynamic topography likely controlled the link to the Arctic Ocean.

The timing of Arctic-Peri-Tethys connections may be hard to constrain using our dynamic topography computations given the temporal resolution and increasing uncertainties back in time. However, the longer trends in seaway configuration seem to correlate well with dynamic topography changes. For example, the dynamic topography anomaly is weaker in the Turgai Strait region during the Paleocene than in the Eocene, which agrees with the closed Paleocene scenario in the paleogeographic maps of Barrier et al. (2018), and is also indicated by faunal migration patterns (Brikiatis, 2014).

4.2. Arctic isolation and a "great" Arctic Ocean in the Eocene

The Arctic Ocean experienced very fresh hydrological conditions during Early-Mid Eocene peaking at ~49–48 Ma recorded by the well documented presence of the *Azolla* freshwater fern (Brinkhuis et al., 2006; Dickson et al., 2022). This has been used to indicate a closed WSS. However, the Arctic Ocean may have been isolated from the global ocean even if the seaway through the Turgai Strait was open in the Eocene.

Our reconstructions show that the oceanic connections between the Tethys and the Eurasian/Paratethys Sea were limited during the Eocene and could have imposed significant restrictions to water exchange between the basins, especially during the Mid Eocene. At the same time, connections between the Eurasian epicontinental Sea, and the North Sea, through the Danish-Polish Through existed episodically (e.g., Palcu and Krijgsman, 2022). We propose that these basins were a part of a greater Arctic Ocean, enabling exchange of water masses and biogeographic dispersal between the Peri-Arctic basins. At its greatest extent, this could have included the Arctic Ocean, Paratethys Sea, North Sea, and the Nordic Seas. Linked through the WSS, the Danish-Polish Trough, and the Barents Sea, and isolated to the South by elevated topography along the Arabian-Eurasian collision zone, Europe, and the Greenland-Scotland Ridge (Fig. 6). Our reconstructions have temporal Tethys-Peri-Tethys connections to the greater Arctic Ocean during the Eocene, also, shallow straits may have existed episodically to the Nordic Seas over the Eastern part of the Greenland-Scotland Ridge (i.e., the Iceland-Faroe Ridge or the Faroe-Shetland Channel) (Straume et al., 2020), and to the North Sea through the Strait of Dover (van Vliet-Lanoë et al., 2010), but there may have been periods of very little water exchange through these straits in the Eocene.

Osmium isotope analysis indicate that seawater exchange rates to the Arctic ocean decreased from the Early Eocene (~ 56 Ma), and reached a minimum ~48–46 Ma, before increasing slightly by 46–44 Ma (Dickson et al., 2022). This does not seem to be directly linked to the WSS, as the seaway is mostly open during this time interval in our reconstructions. The change in Tethys-Peri-Tethys connections along the Southern Eurasian margin may be a more likely cause for the documented changes in water exchange to the Arctic during the Early – Mid Eocene.

Moreover, the WSS was relatively shallow which would not have allowed for much throughflow and could have closed temporarily at several places due to changes in sea level or dynamic topography. There is also a possibility that the Kara Strait (Fig. 1) imposed restrictions to an Arctic connection at this time. Our estimated dynamic topography anomaly is not as negative where the Kara Strait may have existed as in the West Siberian Sea (Figs. 4, 5), and could explain the limited water exchange to the Arctic in the Early-Mid Eocene (Dickson et al., 2022) when there likely was Tethys-Peri Tethys connections (Barrier et al., 2018; Bosboom et al., 2017; Palcu and Krijgsman, 2022; Rögl, 1999) and the Turgai Strait and West Siberian Sea was open (Akhmetiev et al., 2012; Barrier et al., 2018). However, indications of limited water connection at this time cannot be directly inferred from our paleogeography or dynamic topography computations.

5. Summary and conclusions

We generate paleogeographic reconstructions for Eurasia, Arabia and Northern Africa and create a new global paleogeographic DEM covering the Cenozoic time in 1 Myr time intervals. Additionally, we compute time-dependent dynamic topography for the last 100 Myrs and evaluate the role of mantle convection on the paleogeographic evolution of Central Eurasia, and the West Siberian Seaway to the Arctic Ocean.

We find that changes in paleogeography of the West Siberian Seaway correlate well with changes in dynamic topography and that dynamic topography likely played a significant role in the paleogeographic evolution of Central Eurasia. Specifically, changes in an active mantle upwelling below central Eurasia caused changes in dynamic topography and influenced the evolution of the West Siberian Seaway.

Our study shows how deep Earth processes such as mantle convections may have played an important role for regional ocean circulation, climate, and faunal migrations by influencing the paleogeography of a key seaway to the Arctic Ocean.

Data availability

Our global paleogeographic DEMs and dynamic tomography computations are available here: https://doi.org/10.5281/zenodo.8262689. We share the dynamic topography both in a mantle- and paleomagnetic reference frame. Also, visualizations based on this data are available at www.s-ink.org (Crameri et al., 2022).

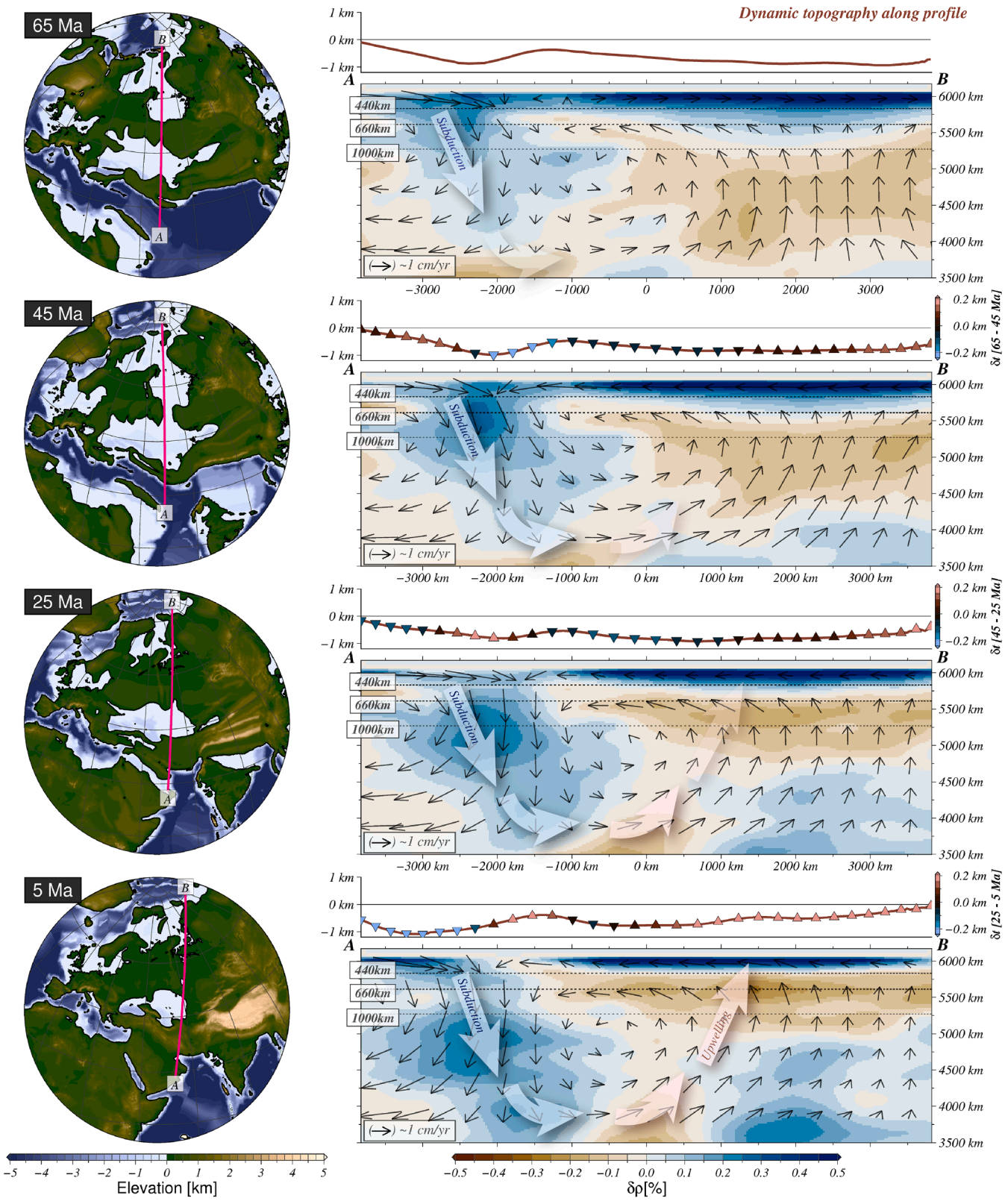

Fig. 5. Cenozoic paleogeography and cross sections showing mantle density anomalies. The orange line shows the dynamic topography along the profile for each time slice, and the colored triangles show the change in dynamic topography from the previous time step indicating mantle induced uplift and subsidence. The density anomalies and dynamic topography are from our model using SMEAN2 tomography. Black arrows show the velocities while the sketched transparent arrows highlight the flow pattern where sinking fast anomalies associated with the Tethyan subduction trigger upwelling beneath Eurasia causing uplift in the region of the West Siberian Seaway. The profile is fixed to Eurasia.

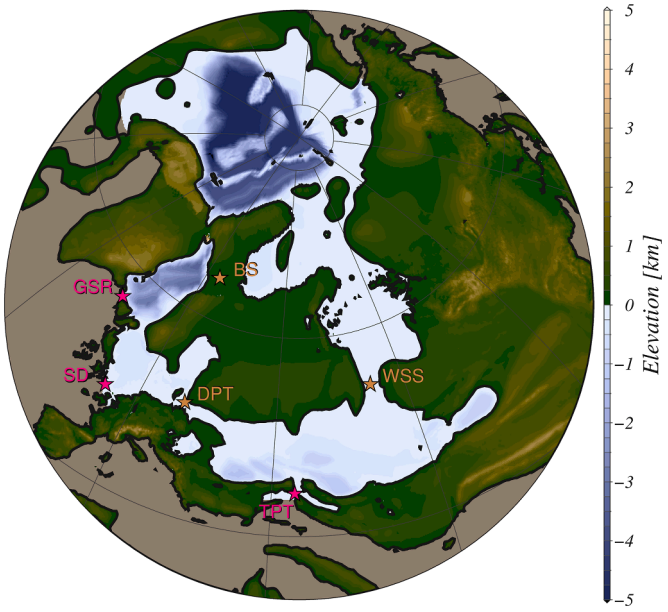

Fig. 6. Extent of the Arctic Ocean in the Mid-Late Eocene (~ 40 Ma). Pink color indicates seaways and straits connecting the Arctic with the global ocean, while orange color indicates internal seaways within the "greater" Arctic Ocean. GSR= Greenland-Scotland Ridge, SD = Strait of Dover, TPT=Tethys Peri-Tethys connections, BS = Barents Sea, DPT=Danish-Polish Through, WSS = West Siberian Seaway.

CRediT authorship contribution statement

Eivind O. Straume: Writing – original draft, Visualization, Methodology, Formal analysis, Data curation, Conceptualization. **Bernhard Steinberger:** Writing – review & editing, Methodology, Formal analysis. **Thorsten W. Becker:** Writing – review & editing, Visualization, Formal analysis, Conceptualization. **Claudio Faccenna:** Writing – review & editing, Conceptualization.

Declaration of competing interest

The authors declare that they have no known competing financial interests or personal relationships that could have appeared to influence the work reported in this paper.

Acknowledgements

Most of this research was conducted while EOS was supported by a Jackson School of Geosciences PLATES-4D Post-Doctoral Scholarship. EOS also acknowledge the support from NRC project 314371 (DOTpaleo). TWB was partially supported by NSF EAR 2045292 and 19214743. B.S acknowledge funding from the Innovation Pool of the Helmholtz Association through the Advanced Earth System Modelling Capacity (ESM) activity. C.F. received funding from Roma Tre Dipartimento di Eccellenza, MIUR. The figures in this paper were generated using Generic Mapping Tools (GMT; Wessel et al., 2019), and perceptually uniform color maps were used to prevent visual distortion of the data (Crameri, 2018).

Supplementary materials

Supplementary material associated with this article can be found, in the online version, at doi:10.1016/j.epsl.2024.118615.

References

Akhmetiev, M.A., Beniamovski, V.N., 2009. Paleogene floral assemblages around epicontinental seas and straits in Northern Central Eurasia: proxies for climatic and paleogeographic evolution. Geol. Acta 7 (1–2), 297–309.
Akhmetiev, M.A., Zaporozhets, N.I., Benyamovskiy, V.N., Aleksandrova, G.N., Iakovleva, A.I., Oreshkina, T.V., 2012. The Paleogene history of the western siberian seaway-a connection of the Peri-Tethys to the arctic ocean. Austrian J. Earth Sci. 105 (1).
Allen, P.A., Armitage, J.J., 2011. Cratonic Basins. Tectonics of Sedimentary Basins, pp. 602–620.
Armitage, J.J., Allen, P.A., 2010. Cratonic basins and the long-term subsidence history of continental interiors. J. Geol. Soc. London 167 (1), 61–70.
Augustin, N., van der Zwan, F.M., Devey, C.W., Brandsdóttir, B., 2021. 13 million years of seafloor spreading throughout the Red Sea Basin. Nat. Commun. 12 (1), 2427.
Barke, J., Abels, H.A., Sangiorgi, F., Greenwood, D.R., Sweet, A.R., Donders, T., Reichart, G.J., Lotter, A.F., Brinkhuis, H., 2011. Orbitally forced Azolla blooms and Middle Eocene Arctic hydrology: clues from palynology. Geology 39 (5), 427–430.
Barrier, E., Vrielynck, B., Brouillet, J.F., and Brunet, .M.F., 2018, Paleotectonic Reconstruction of the Central Tethyan Realm. Tectonono-Sedimentary-Palinspastic Maps from Late Permian to Pliocene.
Beniamovski, V.N., 2007. The Paleogene straits of northern Eurasia. In: Baraboshkin, E.Y. (Ed.), The Cretaceous and Paleogene Straits of Northern Hemisphere. Geological faculty of Moscow State University, pp. 80–118 in Russian.
Bialik, O.M., Frank, M., Betzler, C., Zammit, R., Waldmann, N.D., 2019. Two-step closure of the Miocene Indian Ocean Gateway to the Mediterranean. Sci. Rep. 9 (1), 8842.
Blakey, R., 2021. Paleotectonic and Paleogeographic History of the Arctic region. Atlantic Geol. 57, 7–39.
Bosboom, R., Mandic, O., Dupont-Nivet, G., Proust, J.N., Ormukov, C., Aminov, J., 2017. Late Eocene palaeogeography of the Proto-Paratethys Sea in Central Asia (NW China, Southern Kyrgyzstan and SW Tajikistan). Geological Society, London, Special Publications, pp. 565–588, 427.
Brikiatis, L., 2014. The De Geer, Thulean and Beringia routes: key concepts for understanding early Cenozoic biogeography. J. Biogeogr. 41 (6), 1036–1054.
Brinkhuis, H., Schouten, S., Collinson, M.E., Sluijs, A., Damsté, J.S.S., Dickens, G.R., Huber, M., Cronin, T.M., Onodera, J., Takahashi, K., Bujak, J.P., Stein, R., van der Burgh, J., Eldrett, J.S., Harding, I.C., Lotter, A.F., Sangiorgi, F., Cittert, H.V.K.V., de Leeuw, J.W., Matthiessen, J., Backman, J., Moran, K., the Expedition, S, 2006. Episodic fresh surface waters in the Eocene Arctic Ocean. Nature 441 (7093), 606–609.
Collet, B., Parrot, J.F.O, Taud, H., 2000. Orientation of absolute African plate motion revealed by tomomorphometric analysis of the Ethiopian dome. Geology 28 (12), 1147–1149.
Conrad, C.P., Gurnis, M., 2003. Seismic tomography, surface uplift, and the breakup of Gondwanaland: integrating mantle convection backwards in time. Geochem. Geophys. Geosyst. 4 (3).
Crameri, F., 2018. Scientific colour-maps. Zenodo. https://doi.org/10.5281/zenodo.1243862.
Crameri, F., Shephard, G., and Straume, E.O., 2022, Effective high-quality science graphics from s-Ink. org.
Dickson, A., Davies, M., Bagard, M., Cohen, A., 2022. Quantifying seawater exchange rates in the Eocene Arctic Basin using osmium isotopes. Geochem. Perspect. Lett. 24, 7–11.
Flament, N., Gurnis, M., Müller, R.D., 2013. A review of observations and models of dynamic topography. Lithosphere 5 (2), 189–210.
French, S.W., Romanowicz, B.A., 2014. Whole-mantle radially anisotropic shear velocity structure from spectral-element waveform tomography. Geophys. J. Int. 199 (3), 1303–1327.
Glorie, S., De Grave, J., 2016. Exhuming the Meso–Cenozoic Kyrgyz Tianshan and Siberian Altai-Sayan: a review based on low-temperature thermochronology. Geosci. Front. 7 (2), 155–170.
Goldreich, P., Toomre, A., 1969. Some remarks on polar wandering. J. Geophys. Res. 74 (10), 2555–2567.
Hamon, N., Sepulchre, P., Lefebvre, V., Ramstein, G., 2013. The role of eastern Tethys seaway closure in the Middle Miocene Climatic Transition (ca. 14 Ma). Clim. Past 9 (6), 2687–2702.
Haq, B.U., Al-Qahtani, A.M., 2005. Phanerozoic cycles of sea-level change on the Arabian Platform. GeoArabia 10 (2), 127–160.
Haq, B.U., Hardenbol, J., Vail, P.R., 1987. Chronology of fluctuating sea levels since the Triassic. Science 235 (4793), 1156–1167.
Herold, N., Buzan, J., Seton, M., Goldner, A., Green, J.A.M., Müller, R.D., Markwick, P., Huber, M., 2014. A suite of early Eocene (~ 55 Ma) climate model boundary conditions. Geosci. Model Dev 7 (5), 2077–2090.
Hoggard, M., White, N., Al-Attar, D., 2016. Global dynamic topography observations reveal limited influence of large-scale mantle flow. Nat. Geosci.
Hutchinson, D.K., Coxall, H.K., O'Regan, M., Nilsson, J., Caballero, R., de Boer, A.M., 2019. Arctic closure as a trigger for Atlantic overturning at the Eocene-Oligocene Transition. Nat. Commun. 10 (1), 3797.
Iakovleva, A.I., Brinkhuis, H., Cavagnetto, C., 2001. Late Palaeocene–Early Eocene dinoflagellate cysts from the Turgay Strait, Kazakhstan; correlations across ancient seaways. Palaeogeogr. Palaeoclimatol. Palaeoecol. 172 (3), 243–268.
Jackson, M.G., Konter, J.G., Becker, T.W., 2017. Primordial helium entrained by the hottest mantle plumes. Nature 542 (7641), 340–343.
Kaya, M.Y., Dupont-Nivet, G., Proust, J.N., Roperch, P., Bougeois, L., Meijer, N., Frieling, J., Fioroni, C., Özkan Altıner, S., Vardar, E., Barbolini, N., Stoica, M., Aminov, J., Mamtimin, M., Zhaojie, G., 2019. Paleogene evolution and demise of the

proto-Paratethys Sea in Central Asia (Tarim and Tajik basins): role of intensified tectonic activity at ca. 41 Ma. Basin Res. 31 (3), 461–486.
Lithgow-Bertelloni, C., Gurnis, M., 1997. Cenozoic subsidence and uplift of continents from time-varying dynamic topography. Geology 25 (8), 735–738.
Lu, C., Grand, S.P., Lai, H., Garnero, E.J., 2019. TX2019slab: a new P and S tomography model incorporating subducting slabs. J. Geophys. Res.: Solid Earth 124 (11), 11549–11567.
Lunt, D.J., Bragg, F., Chan, W.L., Hutchinson, D.K., Ladant, J.B., Morozova, P., Niezgodzki, I., Steinig, S., Zhang, Z., Zhu, J., Abe-Ouchi, A., Anagnostou, E., de Boer, A.M., Coxall, H.K., Donnadieu, Y., Foster, G., Inglis, G.N., Knorr, G., Langebroek, P.M., Lear, C.H., Lohmann, G., Poulsen, C.J., Sepulchre, P., Tierney, J. E., Valdes, P.J., Volodin, E.M., Dunkley Jones, T., Hollis, C.J., Huber, M., Otto-Bliesner, B.L., 2021. DeepMIP: model intercomparison of early Eocene climatic optimum (EECO) large-scale climate features and comparison with proxy data. Clim. Past 17 (1), 203–227.
Medvedev, S., Hartz, E.H., Faleide, J.I., 2018. Erosion-driven vertical motions of the circum Arctic: comparative analysis of modern topography. J. Geodyn. 119, 62–81.
Meulenkamp, J.E., Sissingh, W., 2003. Tertiary palaeogeography and tectonostratigraphic evolution of the Northern and Southern Peri-Tethys platforms and the intermediate domains of the African–Eurasian convergent plate boundary zone. Palaeogeogr. Palaeoclimatol. Palaeoecol. 196 (1), 209–228.
Müller, R.D., Flament, N., Cannon, J., Tetley, M.G., Williams, S.E., Cao, X., Bodur, Ö.F., Zahirovic, S., Merdith, A., 2022. A tectonic-rules-based mantle reference frame since 1 billion years ago – implications for supercontinent cycles and plate–mantle system evolution. Solid Earth 13 (7), 1127–1159.
Müller, R.D., Sdrolias, M., Gaina, C., Steinberger, B., Heine, C., 2008. Long-term sea-level fluctuations driven by ocean basin dynamics. Science 319 (5868), 1357–1362.
Okay, A.I., Zattin, M., Cavazza, W., 2010. Apatite fission-track data for the Miocene Arabia-Eurasia collision. Geology 38 (1), 35–38.
Palcu, D.V., Krijgsman, W., 2022. The Dire Straits of Paratethys: Gateways to the Anoxic Giant of Eurasia. Geological Society, London, Special Publications, 523SP523-2021-2073.
Popov, S., Antipov, M., Zastrozhnov, A., Kurina, E., Pinchuk, T., 2010. Sea-level fluctuations on the northern shelf of the Eastern Paratethys in the Oligocene-Neogene. Stratigr. Geol. Correlation 18 (2), 200.
Ramsay, A.T., Smart, C.W., Zachos, J.C., 1998. A Model of Early to Middle Miocene Deep Ocean Circulation For the Atlantic and Indian Oceans. Geological Society, London, Special Publications, pp. 55–70, 131.
Reichow, M.K., Saunders, A.D., White, R.V., Al'Mukhamedov, A.I., Medvedev, A.Y., 2005. Geochemistry and petrogenesis of basalts from the West Siberian Basin: an extension of the Permo–Triassic Siberian Traps, Russia. Lithos 79 (3), 425–452.
Ritsema, J., Deuss, A., van Heijst, H.J., Woodhouse, J.H., 2011. S40RTS: a degree-40 shear-velocity model for the mantle from new Rayleigh wave dispersion, teleseismic traveltime and normal-mode splitting function measurements. Geophys. J. Int. 184 (3), 1223–1236.
Rögl, F., 1997. Palaeogeographic considerations for Mediterranean and Paratethys Seaways (Oligocene to Miocene): annalen des Naturhistorischen Museums in Wien. Serie A für Mineralogie und Petrographie, Geologie und Paläontologie. Anthropol. Prähistorie 99, 279–310.
Rögl, F., 1999. Mediterranean and Paratethys. Facts and hypotheses of an Oligocene to Miocene paleogeography (short overview). Geol. Carpathica 50 (4), 339–349.
Saunders, A.D., England, R.W., Reichow, M.K., White, R.V., 2005. A mantle plume origin for the Siberian traps: uplift and extension in the West Siberian Basin, Russia. Lithos 79 (3), 407–424.
Segev, A., Avni, Y., Shahar, J., Wald, R., 2017. Late Oligocene and Miocene different seaways to the Red Sea–Gulf of Suez rift and the Gulf of Aqaba–Dead Sea basins. Earth. Sci. Rev. 171, 196–219.
Shephard, G.E., Flament, N., Williams, S., Seton, M., Gurnis, M., Müller, R.D., 2014. Circum-Arctic mantle structure and long-wavelength topography since the Jurassic. J. Geophys. Res.: Solid Earth 119 (10), 7889–7908.
Spasojevic, S., Gurnis, M., 2012. Sea level and vertical motion of continents from dynamic earth models since the Late Cretaceous. Am. Assoc. Pet. Geol. Bull. 96 (11), 2037–2064.
Steinberger, B., 2016. Topography caused by mantle density variations: observation-based estimates and models derived from tomography and lithosphere thickness. Geophys. J. Int. 205 (1), 604–621.
Steinberger, B., Calderwood, A.R., 2006. Models of large-scale viscous flow in the Earth's mantle with constraints from mineral physics and surface observations. Geophys. J. Int. 167 (3), 1461–1481.
Steinberger, B., Sutherland, R., O'Connell, R.J., 2004. Prediction of Emperor-Hawaii seamount locations from a revised model of global plate motion and mantle flow. Nature 430 (6996), 167–173.
Steinberger, B., Torsvik, T.H., 2010. Toward an explanation for the present and past locations of the poles. Geochem. Geophys. Geosyst. 11 (6).
Straume, E.O., Gaina, C., Medvedev, S., Hochmuth, K., Gohl, K., Whittaker, J.M., Abdul Fattah, R., Doornenbal, J.C., Hopper, J.R., 2019. GlobSed: updated total sediment thickness in the world's oceans. Geochem. Geophys. Geosyst. 20 (4), 1756–1772.
Straume, E.O., Gaina, C., Medvedev, S., Nisancioglu, K.H., 2020. Global cenozoic paleobathymetry with a focus on the northern hemisphere oceanic gateways. Gondwana Res. 86, 126–143.
Straume, E.O., Nummelin, A., Gaina, C., Nisancioglu, K.H., 2022. Climate transition at the Eocene - Oligocene influenced by bathymetric changes to the Atlantic - Arctic oceanic gateways. Proc. Ntl. Acad. Sci. 119 (17), e2115346119.
Torsvik, T.H., 2016. Tectonic Units of the Earth. In: Cocks, L.R.M., Cocks, L.R.M., Torsvik, T.H. (Eds.), Earth History and Palaeogeography. Cambridge University Press, Cambridge, pp. 38–76.
Torsvik, T.H., Müller, R.D., Van der Voo, R., Steinberger, B., Gaina, C., 2008. Global plate motion frames: toward a unified model. Rev. Geophys. 46 (3).
Torsvik, T.H., Steinberger, B., Shephard, G.E., Doubrovine, P.V., Gaina, C., Domeier, M., Conrad, C.P., Sager, W.W., 2019. Pacific-panthalassic reconstructions: overview, errata and the way forward. Geochem. Geophys. Geosyst. 20 (7), 3659–3689.
Torsvik, T.H., Van der Voo, R., Preeden, U., Mac Niocaill, C., Steinberger, B., Doubrovine, P.V., van Hinsbergen, D.J.J., Domeier, M., Gaina, C., Tohver, E., Meert, J.G., McCausland, P.J.A., Cocks, L.R.M., 2012. Phanerozoic polar wander, palaeogeography and dynamics. Earth. Sci. Rev. 114 (3), 325–368.
van Hinsbergen, D.J.J., de Groot, L.V., van Schaik, S.J., Spakman, W., Bijl, P.K., Sluijs, A., Langereis, C.G., Brinkhuis, H., 2015. A paleolatitude calculator for paleoclimate studies. PLoS One 10 (6), e0126946.
van Hinsbergen, D.J.J., Torsvik, T.H., Schmid, S.M., Maţenco, L.C., Maffione, M., Vissers, R.L.M., Gürer, D., Spakman, W., 2020. Orogenic architecture of the Mediterranean region and kinematic reconstruction of its tectonic evolution since the Triassic. Gondwana Res. 81, 79–229.
van Vliet-Lanoë, B., Gosselin, G., Mansy, J.L., Bourdillon, C., Meurisse-Fort, M., Henriet, J.P., Le Roy, P., Trentesaux, A., 2010. A renewed Cenozoic story of the Strait of Dover. Ann. Soc. Géol. Nord 17 (2), 59–80.
Vetrov, E.V., De Grave, J., Vetrova, N.I., Zhimulev, F.I., Nachtergaele, S., Van Ranst, G., Mikhailova, P.I., 2021. Tectonic evolution of the SE West Siberian Basin (Russia): evidence from apatite fission track thermochronology of its exposed crystalline basement. Minerals 11 (6), 604.
Vibe, Y., Bunge, H.P., Clark, S.R., 2018. Anomalous subsidence history of the West Siberian Basin as an indicator for episodes of mantle induced dynamic topography. Gondwana Res. 53, 99–109.
Vyssotski, A.V., Vyssotski, V.N., Nezhdanov, A.A., 2006. Evolution of the West Siberian Basin. Mar. Pet. Geol. 23 (1), 93–126.
Wessel, P., Luis, J.F., Uieda, L., Scharroo, R., Wobbe, F., Smith, W.H.F., Tian, D., 2019. The generic mapping tools version 6. Geochem. Geophys. Geosyst. 20 (11), 5556–5564.
Williams, C.J.R., Lunt, D.J., Salzmann, U., Reichgelt, T., Inglis, G.N., Greenwood, D.R., Chan, W.L., Abe-Ouchi, A., Donnadieu, Y., Hutchinson, D.K., de Boer, A.M., Ladant, J.B., Morozova, P.A., Niezgodzki, I., Knorr, G., Steinig, S., Zhang, Z., Zhu, J., Huber, M., Otto-Bliesner, B.L., 2022. African hydroclimate during the early eocene from the deepMIP simulations. Paleoceanogr. Paleoclimatol. 37 (5) e2022PA004419.
Xu, X., Lithgow-Bertelloni, C., Conrad, C.P., 2006. Global reconstructions of Cenozoic seafloor ages: implications for bathymetry and sea level. Earth Planet Sci. Lett. 243 (3), 552–564.
Yang, T., Moresi, L., Müller, R.D., Gurnis, M., 2017. Oceanic residual topography agrees with mantle flow predictions at long wavelengths. Geophys. Res. Lett. 44 (21), 10896–10906.
Zhang, Z., Nisancioglu, K., Flatøy, F., Bentsen, M., Bethke, I., Wang, H., 2011. Tropical seaways played a more important role than high latitude seaways in Cenozoic cooling. Climate Past 7 (3), 801–813.